J Sci Comput (2018) 74:1397–1422
https://doi.org/10.1007/s10915-017-0501-0

A C^0 Linear Finite Element Method for Biharmonic Problems

Hailong Guo[1,2] · **Zhimin Zhang**[1,3] · **Qingsong Zou**[4]

Received: 8 December 2016 / Revised: 29 June 2017 / Accepted: 11 July 2017 /
Published online: 20 July 2017

Abstract In this paper, a C^0 linear finite element method for biharmonic equations is constructed and analyzed. In our construction, the popular post-processing gradient recovery operators are used to calculate approximately the second order partial derivatives of a C^0 linear finite element function which do not exist in traditional meaning. The proposed scheme is straightforward and simple. More importantly, it is shown that the numerical solution of the proposed method converges to the exact one with optimal orders both under L^2 and discrete H^2 norms, while the recovered numerical gradient converges to the exact one with a superconvergence order. Some novel properties of gradient recovery operators are discovered in the analysis of our method. In several numerical experiments, our theoretical findings are verified and a comparison of the proposed method with the nonconforming Morley element and C^0 interior penalty method is given.

H. Guo: The research of this author was supported in part by the US National Science Foundation through Grant DMS-1419040. Z. Zhang: The research of this author was supported in part by the following Grants: NSFC 11471031, NSFC 91430216, NASF U1530401, and NSF DMS-1419040. Q. Zou: The research of this author was supported in part by the following Grants: the special project *High performance computing* of National Key Research and Development Program 2016YFB0200604, NSFC 11571384, Guangdong Provincial NSF 2014A030313179, the Fundamental Research Funds for the Central Universities 16lgjc80.

✉ Qingsong Zou
mcszqs@mail.sysu.edu.cn

Hailong Guo
hlguo@math.ucsb.edu

Zhimin Zhang
zmzhang@csrc.ac.cn; zzhang@math.wayne.edu

1 Department of Mathematics, Wayne State University, Detroit, MI 48202, USA

2 Present Address: Department of Mathematics, University of California, Santa Barbara, CA 93106, USA

3 Beijing Computational Science Research Center, Beijing 100193, China

4 School of Data and Computer Science and Guangdong Province Key Laboratory of Computational Science, Sun Yat-sen University, Guangzhou 510275, China

Keywords Biharmonic equation · Gradient recovery · Superconvergence · Linear finite element

Mathematics Subject Classification Primary 65N30; Secondary 45N08

1 Introduction

Gradient recovery technique reconstructs numerical gradients from finite element solutions to achieve a better approximation of gradients of exact solutions. Due to their efficiency and simplicity, some gradient recovery techniques have been widely used in scientific and engineering computation. For instance, the Superconvergence Patch Recovery (SPR) by Zienkiewicz-Zhu [31] has been used in commercial finite element packages such as Abaqus, DiffiPack, Nastran, etc., the Polynomial Preserving Recovery (PPR) by Naga-Zhang has been adopted by COMSOL Multiphysics since 2008 [11,12]. On the other hand, the great success of gradient recovery techniques in practice attracts much attention from the scientific community to establish their mathematical theory, see e.g. [2–5,7,29] and references therein.

In the literature, gradient recovery techniques were used mainly to post-process and to construct a posteriori error estimators. In this paper, we will use gradient recovery techniques to pre-process, namely, to construct numerical schemes from the beginning. Our model problem is the following biharmonic equation

$$\triangle^2 u = f \quad \text{in } \Omega \tag{1.1}$$

$$u = \phi \quad \text{on } \partial\Omega, \tag{1.2}$$

$$\frac{\partial u}{\partial \mathbf{n}} = \psi \quad \text{on } \partial\Omega, \tag{1.3}$$

where $\Omega \subset \mathbb{R}^2$ is a bounded domain, $\mathbf{n}$ is the unit outward normal on the boundary $\partial\Omega$. The boundary condition (1.3) might be replaced by

$$\frac{\partial^2 u}{\partial \mathbf{n}^2} = g \quad \text{on } \partial\Omega. \tag{1.4}$$

Note that finite element methods for biharmonic equations in the literature can be categorized roughly into three different types: conforming, nonconforming, and mixed methods. Due to its complexity in construction and implementation, the conforming method for (1.1) was almost abandoned from scientific and engineering computing since the 1980's. The nonconforming method avoids the complicated construction of C^1 elements, however, its convergence depends heavily on the delicate design of the finite element space see e.g., [1,6,9,10,21]. The mixed methods use continuous Lagrange finite element space. However, it may cause spurious solutions for some problems with simply supported plate boundary conditions, see [28]. Moreover, a mixed method requires solving a saddle point linear system which is more complicated than the symmetric positive definite one derived from a direct discretization of the fourth order operator.

It seems that a method based on the standard variational principle of minimum energy type and involving only nodal degrees of freedom without derivative unknowns would be an ideal choice. In this work, we present and analyze such a method. Let us outline the basic idea. Note that the variational formulation of (1.1)–(1.4) involves the second derivative of the discrete solution, which is impossible to obtain from a direct calculation of C^0 linear element, since the gradient of a function in a C^0 linear finite element space is piecewise

constant (w.r.t the underlying mesh) and discontinuous across each element. To overcome this difficulty, we use the gradient recovery operator G_h to "lift" discontinuous piecewise constant Dv_h to continuous piecewise linear $G_h v_h$, and hence further differentiation $DG_h v_h$ is possible. In other words, we use the special *difference operator* DG_h to discretize the the second order differential operator D^2. Our algorithm for (1.1)–(1.4) is then designed by applying this special *difference operator* to the standard Ritz–Galerkin method. Note that the recovery operator G_h can be defined on a general unstructured grid, and therefore the designed algorithm works for biharmonic problems on an arbitrary geometric domain. On the other hand, comparing with existing conforming and non-conforming methods in the literature, our scheme does not have derivative unknowns. In other words, the total degrees of freedom our scheme is the same as linear element and much less (about 1/4) than the Morley element. and hence is much cheaper. At the same time, we avoid the saddle point problem of mixed methods.

An important contribution of this work is a brand new analysis of the designed scheme. First, we discuss consistency. As indicated in [29], for reasonably regular meshes, $G_h u_I$ is a second-order finite difference scheme of the gradient Du, if u is sufficiently smooth. Here u_I is the interpolation of u in linear finite element space. As a consequence, $DG_h u_I$ approximates $D^2 u$ with convergence order 1, provided u is sufficiently smooth. However, for a discrete function v_h in the finite element space which is not smooth across the element edges, the error $\|Dv_h - G_h v_h\|_0$ is not a small quantity of the high order, sometimes it may not converges to zero at all. Therefore, for functions in the finite element space, we study the consistency error in a weak sense to obtain

$$\left| \int (\nabla v_h - G_h v_h) \cdot \nabla v \right| \lesssim h^i \|v\|_{i+1,\Omega} |G_h v_h|_{1,\Omega}, \, i = 1, 2. \tag{1.5}$$

To the best of our knowledge, this consistency property of the gradient recovery operator has not been thoroughly studied in the literature, and yet it will play a critical role in our error analysis.

Next, we discuss stability. By the construction of the scheme, analysis of (uniform) stability can be reduced to verification of the (uniform) coercivity of the bilinear form $(DG_h \cdot, DG_h \cdot)$ in the following sense

$$\|v_h\|_{0,\Omega} \lesssim \|DG_h v_h\|_{0,\Omega}, \tag{1.6}$$

for all v_h in the finite element space with suitable boundary conditions. We believe that the following stronger (than (1.6)) result

$$\|v_h\|_{0,\Omega} \lesssim \|G_h v_h\|_{0,\Omega}, \tag{1.7}$$

should be valid for all v_h. Recall that $G_h v_h$ is a recovered gradient, we name (1.7) as a *discrete Poincaré inequality*. Here, we would like to mention that although the boundedness

$$\|G_h u_h\|_{0,\Omega} \lesssim |u_h|_{1,\Omega},$$

were studied before, the Poincaré type inequality (1.7) has not been discussed in the literature. The importance of (1.7) can be seen from the following fact that no additional penalty term is needed in order to guarantee the stability, and this fact makes our scheme very simple.

Based on the consistency and stability, we establish error bounds under L^2, H^1, H^2 norms with orders 2, 2, 1, respectively. Note that piecewise linear interpolation error under L^2, H^1, H^2 norms are of order 2, 1, 0, respectively. Therefore, our error estimates are either optimal or superconvergence.

To demonstrate the efficiency of our method, we compare numerically with the Morley element and C^0 interior penalty method. To achieve the same accuracy, we need about one quarter of degrees of freedom of the Morley element and C^0 interior penalty method, since we use only nodal values just as the linear element.

It worths mentioning that gradient recovery operators were used to discretize and solve biharmonic equations by Lamichhane in [18,19]. However, to guarantee the stability and/or *optimal convergence orders* of their corresponding schemes, some additional conditions were enforced on gradient recovery operators. Since popular gradient recovery operators such as SPR and PPR do not satisfy their additional conditions, the application of their method is very limited, and this might be one reason why no numerical example is provided in [18,19]. In this paper, we use popular gradient recovery operators to discretize high order PDEs. This makes our scheme more practical.

At the end of this section, we mention in this paper, the letter C denotes a generic positive constant which may be different at different occurrences. For convenience, the symbols $\lesssim$ will be used in this paper. That $x \lesssim y$ means that $x \leq Cy$ for some constants C that are independent of mesh sizes. Then $x \sim y$ means both $x \lesssim y$ and $y \lesssim x$ hold. And the notation $\|\cdot\|_{i,\Omega}$ and $|\cdot|_{i,\Omega}$ mean the norm and semi-norm respectively in the Sobolev space $H^i(\Omega)$.

2 A Recovery Based Linear FEM

Let $\mathcal{T}_h$ be a *triangulation* of Ω with mesh-size h. We denote by $\mathcal{N}_h$ and $\mathcal{E}_h$ the set of vertices and edges of $\mathcal{T}_h$, respectively. Let V_h be the standard $\mathcal{P}_1$ finite element space corresponding to $\mathcal{T}_h$. It is well-known that $V_h = \text{Span}\{\phi_p : p \in \mathcal{N}_h\}$ with ϕ_p a linear nodal basis corresponding to each vertex $p \in \mathcal{N}_h$. Let $G_h : V_h \longrightarrow V_h \times V_h$ be a gradient recovery operator ([23,31]) defined as below. Given $p \in \mathcal{N}_h$, let the element patch $\omega_p = \cup\{\tau : p \in \bar{\tau}\}$ and define

$$G_h v_h(p) = \frac{1}{|\omega_p|} \int_{\omega_p} \nabla v_h. \tag{2.1}$$

The recovered gradient function is then defined as

$$G_h v_h = \sum_{p \in \mathcal{N}_h} G_h v_h(p) \phi_p.$$

Remark 2.1 There are several popular ways to define $G_h v(p)$ at a vertex $p \in \mathcal{N}_h$ ([23,31]). In the following, two definitions of $G_h v(p)$ other than (2.1) are listed. (a) Local L^2-projection. We seek two polynomials $P_l \in \mathcal{P}^1(\omega_P)$, $(l = x, y)$, such that

$$\int_{\omega_p} [P_l(x, y) - \partial_l v(x, y)] Q(x, y) dx dy = 0, \quad \forall Q \in \mathcal{P}^1(\omega_p), l = x, y, \tag{2.2}$$

and we define

$$G_h v(p) = (P_x(p), P_y(p)).$$

Sometimes, the exact integral in (2.2) is replaced by its discrete counterpart so that the two polynomials $P_l, l = x, y$ satisfying the least-squares fitting equation

$$\sum_{i=1}^{m} [P_l(x_i, y_i) - \partial_l v(x_i, y_i)] Q(x_i, y_i) = 0, \quad \forall Q \in \mathcal{P}^1(\omega_p), l = x, y, \tag{2.3}$$

where $(x_i, y_i), i = 1, \ldots, m$ are m given points in ω_p. (b) The polynomial preserving recovery (PPR). We seek a quadratic function $P \in \mathcal{P}^2(\omega_p)$, such that

$$\sum_{i=1}^{m}[P(x_i, y_i) - v(x_i, y_i)]Q(x_i, y_i) = 0, \quad \forall Q \in \mathcal{P}^2(\omega_P). \tag{2.4}$$

Then we can define $G_h v(p) = (\partial_x P(p), \partial_y P(p))$.

It is known that the above three definitions are equivalent on a mesh of uniform triangular pattern. Here we choose the definition (2.1) only for simplicity of presentation.

Throughout the rest of our paper, we assume that the mesh $\mathcal{T}_h$ is sufficiently regular such that the gradient recovery operator satisfies the following properties:

(a) discrete Poincaré inequality:

$$\text{(A1)} \quad \|v_h\|_{i,\Omega} \lesssim \|G_h v_h\|_{i,\Omega}, \forall v_h \in V_h^0, i = 0, 1$$

where the hidden constants are independent of the mesh size h;

(b) Boundedness:

$$\|G_h v_h\|_{0,\Omega} \lesssim |v_h|_{1,\Omega}, \quad v_h \in V_h; \tag{2.5}$$

(c) Consistency:

$$\|\nabla u - G_h u_I\|_{0,\Omega} \lesssim h^2 \|u\|_{3,\Omega}, \quad u \in H^3(\Omega); \tag{2.6}$$

where u_I is the linear interpolation of u in V_h.

Noticing that G_h is somehow a substitute of ∇ and (A1) will be validated in Sect. 5. (A1) is a reasonable assumption for sufficiently regular meshes. The boundedness property (2.5) holds for most recovery operators [30,31]. Note that the the consistency (2.6) is an improved version of the classic one

$$\|\nabla u - G_h u_I\|_{0,\Omega} \lesssim h^2 |u|_{3,\infty,\Omega}, \quad u \in W^{3,\infty}(\Omega);$$

which has been proved for the PPR in [30] and for the weighted averaging/SPR in [27]. The improved consistency (2.6) is recently shown in [16]. We would like to also mention that for the general boundary condition case, usually a classic operator G_h does not recover the gradient on the boundary as good as that in the interior of the domain. It is shown in [15] that by a suitable modification of the definition of G_h on the boundary nodes, we can construct a recovery operator which has the same convergence rates both on the boundary and in the interior of the domain.

For any given functions α, β defined on $\partial\Omega$, let $V_h^\alpha = \{v \in V_h : v = \alpha_I \text{ on } \partial\Omega\}$ and $V_h^{\alpha\beta} := \{v \in V_h^\alpha \mid G_h v \cdot \mathbf{n} = \beta_I\}$, where α_I, β_I are respectively linear interpolating function of α and β with respect to the mesh $\mathcal{T}_h$, $\mathbf{n}$ is the unit outward normal of $\partial\Omega$. For all $v_h \in V_h$, we have $G_h v_h = (G_h^x v_h, G_h^y v_h) \in V_h \times V_h$ and we denote its derivatives by the matrix

$$D(G_h v_h) = \begin{pmatrix} \partial_x G_h^x v_h & \partial_x G_h^y v_h \\ \partial_y G_h^x v_h & \partial_y G_h^y v_h \end{pmatrix}.$$

For all $v_h, w_h \in V_h$, we define a bilinear form

$$a(v_h, w_h) = \int_\Omega D(G_h v_h) : D(G_h w_h),$$

where the Frobenius product ":" for two matrixes $B_k = (b_{ij}^k)$, $k = 1, 2$ is defined as

$$B_1 : B_2 = \sum_{i,j=1}^{2} b_{ij}^1 b_{ij}^2.$$

The gradient recovery linear element scheme for solving (1.1) reads as : Find $u_h \in V_h^{\phi\psi}$ such that

$$a(u_h, v_h) = (f, v_h), \quad v_h \in V_h^{00}, \tag{2.7}$$

provided the boundary conditions are given by (1.2) and (1.3); and find $u_h \in V_h^{\phi}$, such that

$$a(u_h, v_h) = (f, v_h) + (g, G_h v_h \cdot \mathbf{n})_{\partial\Omega}, \quad v_h \in V_h^0, \tag{2.8}$$

provided the boundary conditions are given by (1.2) and (1.4).

Note that the linear finite element space $V_h \nsubseteq C^1$, both (2.7) and (2.8) can be considered as "nonconforming" methods.

We have the following well-posedness of our algorithms.

Theorem 2.1 *If (A1) holds, both schemes* (2.7) *and* (2.8) *have a unique solution.*

Proof For all $v_h, w_h \in V_h$, by the fact that ∇w_h is piecewise constant with respect to $\mathcal{T}_h$,

$$\begin{aligned}\int_\Omega \nabla w_h \cdot G_h v_h &= \sum_{p\in\mathcal{N}_h} G_h v_h(p) \cdot \int_\Omega \nabla w_h \phi_p \\ &= \sum_{p\in\mathcal{N}_h} G_h v_h(p) \cdot \frac{1}{3}\int_{\omega_p} \nabla w_h \\ &= \frac{1}{3}\sum_{p\in\mathcal{N}_h} |\omega_p| G_h v_h(p) \cdot G_h w_h(p). \end{aligned} \tag{2.9}$$

If $v_h \in V_h^0$, then

$$\begin{aligned}\|G_h v_h\|_0^2 &\sim \frac{1}{3}\sum_{p\in\mathcal{N}_h} |\omega_p| G_h v_h(p)^2 \\ &= \int_\Omega \nabla v_h \cdot G_h v_h = -\int_\Omega v_h \mathrm{div}(G_h v_h).\end{aligned}$$

It follows that

$$\|G_h v_h\|_{0,\Omega}^2 \lesssim \|\mathrm{div}(G_h v_h)\|_{0,\Omega}\|v_h\|_{0,\Omega} \lesssim \|D(G_h v_h)\|_{0,\Omega}\|v_h\|_{0,\Omega}.$$

By (A1), we have

$$\|G_h v_h\|_{0,\Omega} \lesssim \|D(G_h v_h)\|_{0,\Omega} = |G_h v_h|_{1,\Omega}, \forall v_h \in V_h^0. \tag{2.10}$$

In other words, the semi-norm $\|D(G_h \cdot)\|_{0,\Omega} = |G_h \cdot|_{1,\Omega}$ is a norm in V_h^0. Consequently, by the Lax-Milagram theorem, both (2.7) and (2.8) have a unique solution . □

3 Error Analysis

This section is dedicated to a presentation of the convergence and convergence rate analysis of our algorithms.

The properties (2.5) and (2.6) play a critical role in the analysis of the effects of a post-processing procedure done by G_h. To analyze the convergence of our algorithm, we need more properties of G_h such as the assumption (A1) and the following results.

Theorem 3.1 *For all $v_h \in V_h$, $\mathbf{w}_h \in V_h \times V_h$, there holds*

$$\int_\Omega \sum_{p\in\mathcal{N}_h} \mathbf{w}_h(p)\cdot(G_h v_h)(p)\phi_p = \int_\Omega \mathbf{w}_h\cdot\nabla v_h. \tag{3.1}$$

Consequently, if $v \in H^2(\Omega)$ and (A1) holds, then

$$\left|\int_\Omega \nabla v\cdot(G_h v_h - \nabla v_h)\right| \lesssim h\|v\|_{2,\Omega}\|G_h v_h\|_{1,\Omega}; \tag{3.2}$$

if $v \in H^3(\Omega)$ and (A1) holds, then

$$\left|\int_\Omega \nabla v\cdot(G_h v_h - \nabla v_h)\right| \lesssim h^2\|v\|_{3,\Omega}\|G_h v_h\|_{1,\Omega}. \tag{3.3}$$

Proof We first show (3.1). Noticing that $\int_{\omega_p}\phi_p = \frac{1}{3}|\omega_p|$ and that ∇v_h is piecewise constant with respect to $\mathcal{T}_h$, we have that

$$\begin{aligned}
\int_\Omega \sum_{p\in\mathcal{N}_h} \mathbf{w}_h(p)\cdot(G_h v_h)(p)\phi_p &= \sum_{p\in\mathcal{N}_h} \mathbf{w}_h(p)\cdot(G_h v_h)(p)\int_{\omega_p}\phi_p \\
&= \sum_{p\in\mathcal{N}_h} \frac{\mathbf{w}_h(p)}{3}|\omega_p|\cdot(G_h v_h)(p) \\
&= \sum_{p\in\mathcal{N}_h} \frac{\mathbf{w}_h(p)}{3}\cdot\int_{\omega_p}\nabla v_h \\
&= \sum_{\tau\in\mathcal{T}_h}\int_\tau\left(\sum_{p\in\mathcal{N}_h\cap\tau}\frac{\mathbf{w}_h(p)}{3}\right)\cdot\nabla v_h \\
&= \sum_{\tau\in\mathcal{T}_h}\int_\tau \mathbf{w}_h\cdot\nabla v_h = \int_\Omega \mathbf{w}_h\cdot\nabla v_h.
\end{aligned}$$

We next use (3.1) to show (3.2) and (3.3). For all $v \in H^2(\Omega)$, let $(\nabla v)_I \in V_h$ be the standard Lagrange interpolating operator of ∇v. Then

$$\|\nabla v - (\nabla v)_I\|_{0,\Omega} \lesssim h\|v\|_{2,\Omega}.$$

By (3.1),

$$\int_\Omega \sum_{p\in\mathcal{N}_h} (\nabla v)_I(p)\cdot(G_h v_h)(p)\phi_p = \int_\Omega (\nabla v)_I\cdot\nabla v_h,$$

therefore,

$$\int_\Omega \nabla v\cdot(G_h v_h - \nabla v_h) = \sum_{p\in\mathcal{N}_h}\int_{\omega_p}(\nabla v - (\nabla v)_I(p))\cdot(G_h v_h)(p)\phi_p - \int_\Omega(\nabla v - (\nabla v)_I)\cdot\nabla v_h. \tag{3.4}$$

Next, we estimate separately the two terms on the right-hand side of the above equality.

For the second term, we have

$$\left|\int_\Omega (\nabla v - (\nabla v)_I)\cdot \nabla v_h\right| \lesssim h\|v\|_{2,\Omega}|v_h|_{1,\Omega} \lesssim h\|v\|_{2,\Omega}|G_h v_h|_{1,\Omega},\ v\in H^2, \quad (3.5)$$

$$\left|\int_\Omega (\nabla v - (\nabla v)_I)\cdot \nabla v_h\right| \lesssim h^2\|v\|_{3,\Omega}|v_h|_{1,\Omega} \lesssim h\|v\|_{3,\Omega}|G_h v_h|_{1,\Omega},\ v\in H^3. \quad (3.6)$$

Here we used (A1) at the last step.

For the first term, since $\nabla v\cdot G_h v_h \in H^1$ and $\sum_{p\in\mathcal{N}_h}\mathbf{v}(p)\cdot G_h v_h(p)\phi_p$ is the linear interpolation of $\nabla v\cdot G_h v_h$, we have

$$\begin{aligned}
&\left|\sum_{p\in\mathcal{N}_h}\int_{\omega_p}(\nabla v - (\nabla v)_I(p))\cdot(G_h v_h)(p)\phi_p\right| \\
&= \left|\int_\Omega\left(\nabla v\cdot G_h v_h - \sum_{p\in\mathcal{N}_h}\mathbf{v}(p)\cdot G_h v_h(p)\phi_p\right)\right| \\
&= \left|\int_\Omega\left(\nabla v\cdot G_h v_h - (\nabla v\cdot G_h v_h)_I\right)\right| \\
&\lesssim \|\nabla v\cdot G_h v_h - (\nabla v\cdot G_h v_h)_I\|_{0,\Omega}\,.
\end{aligned}$$

If $v\in H^2$, then $\nabla v\cdot G_h v_h\in H^1$ and thus we have

$$\|\nabla v\cdot G_h v_h - (\nabla v\cdot G_h v_h)_I\|_{0,\Omega} \lesssim h|\nabla v\cdot G_h v_h|_{1,\Omega} \lesssim h\|v\|_{2,\Omega}\|G_h v_h\|_{1,\Omega}.$$

That is, we have

$$\left|\sum_{p\in\mathcal{N}_h}\int_{\omega_p}(\nabla v - (\nabla v)_I(p))\cdot(G_h v_h)(p)\phi_p\right| \lesssim h\|v\|_{2,\Omega}\|G_h v_h\|_{1,\Omega}. \quad (3.7)$$

The estimate (3.2) follows by substituting (3.5) and (3.7) into the right-hand side of (3.4).

If $v\in H^3$, we denote the broken Sobolev space by

$$H^2_{\mathcal{T}_h}(\Omega) = \{w\in H^1(\Omega)\cap C(\Omega) : w|_\tau \in H^2(\tau), \tau\in\mathcal{T}_h\}.$$

Then for all $w\in H^2_{\mathcal{T}_h}(\Omega)$, we have

$$\|w - w_I\|_{0,\tau} \lesssim h^2|w|_{2,\tau},\quad \forall\tau\in\mathcal{T}_h.$$

Since $v\in H^3(\Omega)$, $\nabla v\cdot G_h v_h\in H^2_{\mathcal{T}_h}(\Omega)$. Therefore

$$\begin{aligned}
\|\nabla v G_h v_h - (\nabla v G_h v_h)_I\|^2_{0,\Omega} &= \sum_{\tau\in\mathcal{T}_h}\|\nabla v G_h v_h - (\nabla v G_h v_h)_I\|^2_{0,\tau} \\
&\lesssim h^4\sum_{\tau\in\mathcal{T}_h}|\nabla v\cdot G_h v_h|^2_{2,\tau} \\
&\lesssim h^4\sum_{\tau\in\mathcal{T}_h}\|v\|^2_{3,\tau}\|G_h v_h\|^2_{1,\tau} \\
&\lesssim h^4\|v\|^2_{3,\Omega}\|G_h v_h\|^2_{1,\Omega}.
\end{aligned}$$

Then we have

$$\left| \sum_{p\in\mathcal{N}_h} \int_{\omega_p} (\nabla v - (\nabla v)_I(p)) \cdot (G_h v_h)(p)\phi_p \right| \lesssim h^2 \|v\|_{3,\Omega} \|G_h v_h\|_{1,\Omega}. \tag{3.8}$$

The estimate (3.3) follows by substituting (3.8) and (3.5) into the right-hand side of (3.4). □

Remark 3.1 The inequalities (3.2) and (3.3) are estimates of the error $\nabla v_h - G_h v_h$ in a weak sense. Note that $\|\nabla v_h - G_h v_h\|_{0,\Omega}$ is not necessary of $\mathcal{O}(h)$ for all $v_h \in V_h$. In the next section, we will use (3.2) to analyze the H^2 error of the discrete solution u_h and use (3.3) to analyze the H^1 error of u_h.

3.1 H^2 Error Estimate

We first establish the H^2 error bound.

Theorem 3.2 *Let u_h be the solution of (2.7) or (2.8). If $u \in H^4$ and the mesh $\mathcal{T}_h$ is sufficient small such that (A1) holds, then*

$$\|DG_h(u_h - u_I)\|_{0,\Omega} \lesssim h\|u\|_{4,\Omega}, \tag{3.9}$$

where u_I is the linear interpolation of u in V_h. Consequently,

$$\|D^2 u - DG_h u_h\|_{0,\Omega} \lesssim h\|u\|_{4,\Omega}. \tag{3.10}$$

Proof We first show that

$$a(u_h - u_I, v_h) = (\nabla(\triangle u), G_h v_h - \nabla v_h) + \int_\Omega (D^2 u - DG_h u_I) : DG_h v_h \tag{3.11}$$

holds for all $v_h \in V_h^{00}$ provided u_h is a solution of (2.7) and it holds for all $v_h \in V_h^0$ provided u_h is a solution of (2.8). In fact, when u_h is the solution of (2.7), for any $v_h \in V_h^{00}$,

$$\begin{aligned} a(u_h - u_I, v_h) &= a(u_h, v_h) - a(u_I, v_h) \\ &= (f, v_h) - a(u_I, v_h) = (\triangle^2 u, v_h) - a(u_I, v_h) \\ &= -(\nabla(\triangle u), \nabla v_h) - a(u_I, v_h) \\ &= (\nabla(\triangle u), G_h v_h - \nabla v_h) - (\nabla(\triangle u), G_h v_h) - a(u_I, v_h) \\ &= (\nabla(\triangle u), G_h v_h - \nabla v_h) + \int_\Omega (D^2 u - DG_h u_I) : DG_h v_h; \end{aligned}$$

when u_h is the solution of (2.8), for any $v_h \in V_h^0$,

$$\begin{aligned} a(u_h - u_I, v_h) &= a(u_h, v_h) - a(u_I, v_h) \\ &= (f, v_h) + (g, G_h v_h \cdot \mathbf{n})_{\partial\Omega} - a(u_I, v_h) \\ &= -(\nabla(\triangle u), \nabla v_h) + (g, G_h v_h \cdot \mathbf{n})_{\partial\Omega} - a(u_I, v_h) \\ &= (\nabla(\triangle u), G_h v_h - \nabla v_h) + \int_\Omega (D^2 u - DG_h u_I) : DG_h v_h. \end{aligned}$$

Next we estimate the right-hand side of (3.11). First, by (3.2),

$$|(\nabla(\triangle u), G_h v_h - \nabla v_h)| \lesssim h\|u\|_{4,\Omega}\|G_h v_h\|_{1,\Omega} \lesssim h\|u\|_4 |G_h v_h|_{1,\Omega}, \tag{3.12}$$

where in the last inequality, we used the equivalence $\|G_h v_h\|_{1,\Omega} \sim |G_h v_h|_{1,\Omega}$, $v_h \in V_h^0$. Secondly, for all $\mathbf{w}_h \in V_h \times V_h$,

$$\begin{aligned}\|D^2 u - D(G_h u_I)\|_{0,\Omega} &\le \|D^2 u - D\mathbf{w}_h\|_{0,\Omega} + \|D\mathbf{w}_h - D(G_h u_I))\|_{0,\Omega} \\ &\le \|D^2 u - D\mathbf{w}_h\|_{0,\Omega} + h^{-1}\|\mathbf{w}_h - G_h(u_I)\|_{0,\Omega}.\end{aligned}$$

We choose $\mathbf{w}_h = (\nabla u)_I$, then $\|\nabla u - \mathbf{w}_h\|_{0,\Omega} \lesssim h^2\|u\|_{4,\Omega}$ and $\|D^2 u - D\mathbf{w}_h\|_{0,\Omega} \lesssim h\|u\|_{4,\Omega}$. Noticing (2), we obtain $\|\mathbf{w}_h - G_h u_I\|_{0,\Omega} \lesssim h^2\|u\|_{4,\Omega}$. Consequently, we have

$$\|D^2 u - D(G_h u_I)\|_{0,\Omega} \lesssim h\|u\|_{4,\Omega}, \tag{3.13}$$

and hence,

$$\left|\int_\Omega (D^2 u - DG_h u_I) : DG_h v_h\right| \lesssim h\|u\|_{4,\Omega}|G_h v_h|_{1,\Omega}. \tag{3.14}$$

Substituting (3.12)–(3.14) into (3.11), we obtain

$$a(u_h - u_I, v_h) \lesssim h\|u\|_4|G_h v_h|_{1,\Omega} = h\|u\|_{4,\Omega}\|DG_h v_h\|_{0,\Omega}. \tag{3.15}$$

Note that when u_h is the solution of (2.7), $u_h, u_I \in V_h^{\phi\psi}$, thus $u_h - u_I \in V_h^{00}$. When u_h is the solution of (2.8), we have $u_h - u_I \in V_h^0$. In other words, we can always choose $v_h = u_h - u_I$ in (3.15) from which (3.9) follows. The estimate (3.10) is a direct consequence of (3.9) and (3.13). □

3.2 H^1 Error Estimate

In this section, we use the Aubin–Nitsche technique to estimate the H^1 norm error $\|\nabla u - G_h u_h\|_{0,\Omega}$. To this end, we construct the following auxiliary problems :

(1) If the boundary conditions are given by (1.2) and (1.3), find $U \in H_0^2(\Omega)$ such that for all $v \in H_0^2(\Omega)$,

$$\int_\Omega D^2 U : D^2 v = (G_h(u_h - u_I), \nabla v); \tag{3.16}$$

If the boundary conditions are given by (1.2) and (1.4), find $U \in H_0^1(\Omega)$ such that for all $v \in H_0^1(\Omega)$, (3.16) holds.

(2) If the boundary conditions are given by (1.2) and (1.3), find $U_h \in V_h^{00}$ such that for all $v_h \in V_h^{00}$,

$$a(U_h, v_h) = (G_h(u_h - u_I), \nabla v_h); \tag{3.17}$$

If the boundary conditions are given by (1.2) and (1.4), find $U_h \in V_h^0$ such that for all $v_h \in V_h^0$, (3.17) holds.

It is easy to deduce from (3.16) that

$$\|U\|_{3,\Omega} \lesssim \|G_h(u_h - u_I)\|_{0,\Omega}, \tag{3.18}$$

Moreover, since the equation (3.17) is a discrete counterpart of (3.16), we can have

$$\|D(G_h U_h)\|_{0,\Omega} \lesssim \|G_h(u_h - u_I)\|_{0,\Omega}. \tag{3.19}$$

Theorem 3.3 *Let u_h be a solution of (2.7) or (2.8). If the mesh is sufficient regular such that (A1) and (2) hold, then*

$$\|G_h(u_h - u_I)\|_{0,\Omega} \lesssim h^2\|u\|_{5,\Omega}. \tag{3.20}$$

Consequently,

$$\|\nabla u - G_h u_h\|_{0,\Omega} \lesssim h^2\|u\|_{5,\Omega}. \tag{3.21}$$

Proof First, by the definition of the auxiliary problems and (3.11), we have

$$\begin{aligned}(G_h(u_h - u_I), \nabla(u_h - u_I)) &= a(U_h, u_h - u_I) = a(u_h - u_I, U_h)\\ &= (\nabla(\triangle u), G_h U_h - \nabla U_h) + \int_\Omega (D^2 u - DG_h u_I) : DG_h U_h\\ &= I_1 + I_2 + I_3,\end{aligned}$$

where

$$\begin{aligned}I_1 &= (\nabla(\triangle u), G_h U_h - \nabla U_h),\\ I_2 &= \int_\Omega (D^2 u - DG_h u_I) : D^2 U,\\ I_3 &= -\int_\Omega (D^2 u - DG_h u_I) : (D^2 U - DG_h U_h).\end{aligned}$$

We first estimate I_1. By (3.3) and (3.19),

$$\begin{aligned}I_1 &\lesssim h^2 \|u\|_{5,\Omega} \|DG_h U_h\|_{0,\Omega}\\ &\lesssim h^2 \|u\|_{5,\Omega} \|G_h(u_h - u_I)\|_{0,\Omega}.\end{aligned}$$

Moreover,

$$\begin{aligned}|I_2| &= \left| \int_\Omega (Du - G_h u_I) \cdot \nabla(\triangle U) \right|\\ &\lesssim h^2 \|u\|_{4,\Omega} \|U\|_{3,\Omega}\\ &\lesssim h^2 \|u\|_{4,\Omega} \|G_h(u_h - u_I)\|_{0,\Omega}.\end{aligned}$$

Finally, by Cauchy-Schwartz inequality,

$$\begin{aligned}|I_3| &= \|D^2 u - DG_h u_I)\|_{0,\Omega} \|D^2 U - DG_h U_h\|_{0,\Omega}\\ &\lesssim h^2 \|u\|_{4,\Omega} \|G_h(u_h - u_I)\|_{0,\Omega}.\end{aligned}$$

Summarizing all the above estimates, we obtain

$$(G_h(u_h - u_I), \nabla(u_h - u_I)) \lesssim h^2 \|u\|_{5,\Omega} \|G_h(u_h - u_I)\|_{0,\Omega}.$$

Noticing that

$$\|G_h(u_h - u_I)\|_{0,\Omega}^2 \sim \frac{1}{3} \sum_{p \in \mathcal{N}_h} (G_h(u_h - u_I)(p))^2 |\omega_p| = (G_h(u_h - u_I), \nabla(u_h - u_I)),$$

the estimate (3.20) follows.

The H^1 error estimate of (3.21) is a direct consequence of (3.20) and (2). □

3.3 L^2 Error Estimate

Theorem 3.4 *Let u_h be a solution of (2.7) or (2.8). If the mesh is sufficient regular such that (A1) and (2) hold, then*

$$\|u - u_h\|_{0,\Omega} \lesssim h^2 \|u\|_{5,\Omega}. \tag{3.22}$$

Proof By the assumption (A1) and (3.9),

$$\|u_I - u_h\|_{0,\Omega} \lesssim \|G_h(u_I - u_h)\|_{0,\Omega} \lesssim h^2 \|u\|_{5,\Omega}.$$

Then

$$\|u - u_h\|_{0,\Omega} \lesssim \|u - u_I\|_{0,\Omega} + \|u_I - u_h\|_{0,\Omega} \lesssim h^2 \|u\|_{5,\Omega}.$$

□

4 Validity of the Assumption (A1)

In this section, we provide a proof of the assumption of (A1).

4.1 Validity of the Assumption (A1) on an Uniform Mesh

First, we validate (A1) for a special case in which Ω is a rectangular domain and T_h is a mesh of the uniform triangular pattern. Precisely, let $\Omega = [a, b] \times [c, d]$ and $x_i = a + \frac{i}{M}(b-a)$, $i = 0, \ldots, M$, $y_j = c + \frac{j}{N}(d-c)$, $j = 0, \ldots, N$. Let $h = \max\{h_x, h_y\}$, $h_x = \frac{b-a}{M}$, $h_y = \frac{d-c}{N}$ be the mesh size and $\mathcal{T}_h$ be the partition obtained by dividing each rectangle $[x_i, x_{i+1}] \times [y_j, y_{j+1}]$, $i = 0, \ldots, M-1$, $j = 0, \ldots, N-1$ into two triangles $\triangle p_{ij} p_{i+1,j} p_{i+1,j+1}$ and $\triangle p_{i+1,j+1} p_{i,j+1} p_{ij}$ with $p_{ij} = (x_i, y_j)$, see Fig. 1.

For a given $v_h \in V_h$ and a vertex $p = p_{ij}$, $0 \le i, j \le N$, we denote $v_{ij} = v_h(p_{ij})$ and $G_{ij} = (G_{ij}^x, G_{ij}^y) = G_h v_h(p_{ij})$ for simplicity. We next derive the representation of G_{ij} in terms of v_{ij}. A simple calculation of (2.1) yields that if $1 \le i \le M-1$, $1 \le j \le N-1$,

$$\begin{aligned} 6G_{ij} = {} & (v_{i+1,j+1} - v_{i-1,j-1}) \begin{pmatrix} h_x^{-1} \\ h_y^{-1} \end{pmatrix} \\ & + (v_{i,j+1} - v_{i,j-1}) \begin{pmatrix} -h_x^{-1} \\ 2h_y^{-1} \end{pmatrix} \\ & + (v_{i+1,j} - v_{i-1,j}) \begin{pmatrix} 2h_x^{-1} \\ -h_y^{-1} \end{pmatrix}. \end{aligned} \tag{4.1}$$

Moreover,

$$G_{00} = v_{11} \begin{pmatrix} h_x^{-1} \\ h_y^{-1} \end{pmatrix}, G_{M0} = G_{0N} = 0, G_{MN} = -v_{M-1,N-1} \begin{pmatrix} h_x^{-1} \\ h_y^{-1} \end{pmatrix},$$

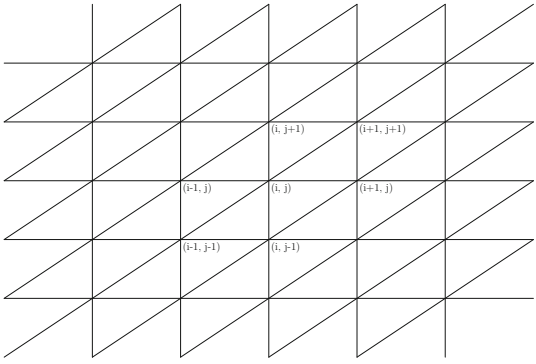

Fig. 1 A regular mesh

and for $1 \le i \le M-1$,

$$3G_{i0} = v_{i+1,1}\begin{pmatrix} h_x^{-1} \\ h_y^{-1} \end{pmatrix} + v_{i1}\begin{pmatrix} -h_x^{-1} \\ 2h_y^{-1} \end{pmatrix},$$
$$3G_{iN} = -v_{i-1,N-1}\begin{pmatrix} h_x^{-1} \\ h_y^{-1} \end{pmatrix} - v_{i,N-1}\begin{pmatrix} -h_x^{-1} \\ 2h_y^{-1} \end{pmatrix},$$

for $1 \le j \le N-1$,

$$3G_{0j} = v_{1,j+1}\begin{pmatrix} h_x^{-1} \\ h_y^{-1} \end{pmatrix} + v_{1j}\begin{pmatrix} 2h_x^{-1} \\ -h_y^{-1} \end{pmatrix},$$
$$3G_{Mj} = -v_{M-1,j-1}\begin{pmatrix} h_x^{-1} \\ h_y^{-1} \end{pmatrix} - v_{M-1,j}\begin{pmatrix} 2h_x^{-1} \\ -h_y^{-1} \end{pmatrix}.$$

Note that by (4.1), it is easy to obtain that

$$v_{ij} + v_{i+1,j+1} = v_{i+1,j-1} + v_{i+2,j} - 2h_x G^x_{i+1,j} + 2h_y G^y_{i+1,j},$$
$$v_{i,j+1} + v_{i+1,j+1} = v_{i-1,j-1} + v_{i,j-1} + 4h_x G^x_{ij} + 2h_y G^y_{ij},$$
$$v_{i,j+1} + v_{ij} = v_{i-2,j} + v_{i-2,j-1} + 2h_x G^x_{i-1,j} + 4h_y G^y_{i-1,j}.$$

Letting $k_1 = \min(M-i-1, j)$, $k_2 = \min(i, j/2)$, $k_3 = \min(i/2, j)$, we recursively have

$$v_{ij} + v_{i+1,j+1} = v_{i+k_1,j-k_1} + v_{i+k_1+1,j-k_1+1} - 2\sum_{k=1}^{k_1}(h_x G^x_{i+k,j+1-k} - h_y G^y_{i+k,j+1-k}),$$
$$\begin{aligned} v_{i,j+1} + v_{i+1,j+1} &= v_{i-k_2,j-2k_2+1} + v_{i+1-k_2,j-2k_2+1} \\ &\quad + 2\sum_{k=1}^{k_2}(h_x G^x_{i+1-k,j-2k} + 2h_y G^y_{i+1-k,j-2k}), \end{aligned}$$
$$v_{i,j+1} + v_{ij} = v_{i-2k_3,j+1-k_3} + v_{i-2k_3,j-k_3} + 2\sum_{k=1}^{k_3}(2h_x G^x_{i-2k+1,j-k} + h_y G^y_{i-2k+1,j-k}).$$

Consequently, we have

$$\begin{aligned} 2v_{ij} &= v_{i+k_1,j-k_1} + v_{i+k_1+1,j-k_1+1} - 2\sum_{k=1}^{k_1}(h_x G^x_{i+k,j+1-k} - h_y G^y_{i+k,j+1-k}) \\ &\quad - \left(v_{i-k_2,j-2k_2+1} + v_{i+1-k_2,j-2k_2+1} + 2\sum_{k=1}^{k_2}(h_x G^x_{i+1-k,j-2k} + 2h_y G^y_{i+1-k,j-2k}) \right) \\ &\quad + v_{i-2k_3,j+1-k_3} + v_{i-2k_3,j-k_3} + 2\sum_{k=1}^{k_3}(2h_x G^x_{i-2k+1,j-k} + h_y G^y_{i-2k+1,j-k}). \end{aligned} \tag{4.2}$$

On the other hand, for all $1 \le i \le M-1$, it is easy to obtain that

$$v_{i1} = 2(h_y g^y_{i0} - h_x g^x_{i0}),\ v_{i,N-1} = 2(h_x g^x_{iN} - h_y g^y_{iN});$$

and for all $1 \le j \le N-1$,

$$v_{1j} = 2(h_x g^x_{0j} - h_y g^y_{0j}),\ v_{M-1,j} = 2(h_y g^y_{Mj} - h_x g^x_{Mj}).$$

Summarizing the above calculations, we obtain that for $v_h \in V_h^0$,

$$v_{ij} = \sum_{(i',j')\in\mathcal{N}_{ij}} \mathbf{b}_{ij,i'j'} \cdot G_{i'j'}. \tag{4.3}$$

with the vectorial coefficients satisfying

$$|\mathbf{b}_{ij,i'j'}| \sim h, \#\mathcal{N}_{ij} \lesssim h^{-1}.$$

Consequently,

$$|v_{ij}|^2 \lesssim h \left(\sum_{(i',j')\in\mathcal{N}_{ij}} |G_{i'j'}|^2 \right).$$

Therefore, noticing $|\omega_{ij}| \sim h^2$,

$$\begin{aligned}
\|v_h\|_{0,\Omega}^2 &\sim \sum_{0\le i\le M, 0\le j\le N} v_{ij}^2 |\omega_{ij}| \\
&\lesssim h^3 \sum_{0\le i\le M, 0\le j\le N} \left(\sum_{(i',j')\in\mathcal{N}_{ij}} |G_{i'j'}|^2 \right) \\
&\lesssim h \sum_{0\le i'\le M, 0\le j'\le N} |G_{i'j'}|^2 |\omega_{i'j'}| \left(\sum_{\mathcal{N}_{ij}\ni(i',j')} 1 \right) \\
&\lesssim \sum_{0\le i'j'\le M, 0\le j\le N} |G_{i'j'}|^2 |\omega_{i'j'}| \sim \|G_h v_h\|_{0,\Omega}^2
\end{aligned}$$

Similarly, we have

$$\begin{aligned}
|v_{ij} - v_{i,j+1}|^2 &\lesssim h \left(\sum_{(i',j')\in\mathcal{N}_{ij}} |G_{i'j'} - G_{i',j'+1}|^2 \right), \\
|v_{ij} - v_{i+1,j}|^2 &\lesssim h \left(\sum_{(i',j')\in\mathcal{N}_{ij}} |G_{i'j'} - G_{i'+1,j'}|^2 \right), \\
|v_{ij} - v_{i+1,j+1}|^2 &\lesssim h \left(\sum_{(i',j')\in\mathcal{N}_{ij}} |G_{i'j'} - G_{i'+1,j'+1}|^2 \right).
\end{aligned}$$

Then

$$\begin{aligned}
|v_h|_{1,\Omega}^2 &\sim \sum_{0\le i\le M-1, 0\le j\le N-1} (v_{ij} - v_{i,j+1})^2 + |v_{ij} - v_{i+1,j}|^2 + |v_{ij} - v_{i+1,j+1}|^2 \\
&\lesssim h \sum_{0\le i\le M-1, 0\le j\le N-1} \left(\sum_{(i',j')\in\mathcal{N}_{ij}} |G_{i'j'} - G_{i',j'+1}|^2 + |G_{i'j'} - G_{i'+1,j'}|^2 + |G_{i'j'} - G_{i'+1,j'+1}|^2 \right) \\
&\lesssim \sum_{0\le i'\le M-1, 0\le j'\le N-1} |G_{i'j'} - G_{i',j'+1}|^2 + |G_{i'j'} - G_{i'+1,j'}|^2 + |G_{i'j'} - G_{i'+1,j'+1}|^2 \\
&\sim \|G_h v_h\|_{1,\Omega}^2.
\end{aligned}$$

Namely, we have verified (A1) for this special grid $\mathcal{T}_h$.

4.2 Validity of the Assumption (A1) on a More General Mesh

In this subsection, we validate (A1) for a case that the underlying mesh is a small random perturbation of a uniform mesh.

For $i = 1, 2$, let $\mathcal{T}_h^i = \left\{T_j^i : j = 1, \ldots, m\right\}$ be two shape-regular and quasi-uniform triangulations of Ω. Furthermore, let $\mathcal{N}_h^i = \left\{p_j^i : j = 1, \ldots, n\right\}$ be the sets of all nodes of $\mathcal{T}_h^i$. Without loss of generality, we may assume

$$\operatorname{dist}(p_j^1, p_j^2) < \epsilon \tag{4.4}$$

for all $p_j^i \in \mathcal{N}_h^i$ and given $\epsilon > 0$.

Let V_h^i be the linear finite element space on the mesh $\mathcal{T}_h^i$ and $V_{h,0}^i = V_h^i \cap H_0^1(\Omega)$. For any vector $\mathbf{v} = (v_1, \ldots, v_n) \in \mathbb{R}^n$, define $v^i = \sum_{j=1}^n v_j \phi_j^i \in V_h^i$, where $\{\phi_j^i\}_{j=1}^n$ are the standard nodal basis functions in the finite element space V_h^i. When ϵ is sufficiently small, (4.4) implies that

$$|\omega_1 \setminus \omega_2|, |\omega_2 \setminus \omega_1| \lesssim \epsilon |\omega_i|, i = 1, 2 \tag{4.5}$$

$$\|\phi_j^1 - \phi_j^2\|_{0,\infty,\omega_j^1 \cup \omega_j^2} \lesssim \epsilon, \forall j, \tag{4.6}$$

and

$$\|\nabla \phi_j^1 - \nabla \phi_j^2\|_{0,\infty,\omega_j^1 \cup \omega_j^2} \lesssim \epsilon h^{-1}, \forall j, \tag{4.7}$$

where ω_j^i is the support of the basis function v_j^i and $|\omega_j^i|$ is the measure of ω_j^i. As a direct consequence,

$$\|v^1 - v^2\|_{0,\Omega} \lesssim \epsilon \|v^i\|_{0,\Omega}, i = 1, 2, \tag{4.8}$$

and

$$\|\nabla v^1 - \nabla v^2\|_{0,\Omega} \lesssim \epsilon h^{-1} \|v^i\|_{0,\Omega}, i = 1, 2. \tag{4.9}$$

Moreover, noticing that

$$(G_h^i v^i)(p_j^i) = \frac{1}{|w_j^i|} \int_{w_j^i} \nabla v^i dx,$$

we have

$$\begin{aligned}(G_h^1 v^1)(p_j^1) - (G_h^2 v^2)(p_j^2) =& \frac{1}{|w_j^1|} \int_{\omega_1 \cap \omega_2} (\nabla v^1 - \nabla v^2) \\ &+ \frac{1}{|w_j^1|} \int_{\omega_1 \setminus \omega_2} \nabla v^1 - \frac{1}{|w_j^2|} \int_{\omega_2 \setminus \omega_1} \nabla v^2 \\ &+ \frac{1}{|w_j^1|} \int_{\omega_1 \cap \omega_2} \nabla v^2 - \frac{1}{|w_j^2|} \int_{\omega_1 \cap \omega_2} \nabla v^2.\end{aligned}$$

Thus by (4.5)–(4.9),

$$\begin{aligned}|G_h^1 v^1)(p_j^1) - G_h^2 v^2)(p_j^2)| \lesssim & \frac{1}{|w_j^1|}\|\nabla v^1 - \nabla v^2\|_{0,\omega_1\cap\omega_2}|\omega_1\cap\omega_2|^{\frac{1}{2}} \\ & + \frac{1}{|w_j^1|}\|\nabla v^1\|_{\omega_1\setminus\omega_2}|\omega_1\setminus\omega_2|^{\frac{1}{2}} + \frac{1}{|w_j^2|}\|\nabla v^2\|_{\omega_2\setminus\omega_1}|\omega_1\setminus\omega_2|^{\frac{1}{2}} \\ & + |\frac{1}{|w_j^1|} - \frac{1}{|w_j^2|}|\|\nabla v^2\|_{0,\omega_1\cap\omega_2}|\omega_1\cap\omega_2|^{\frac{1}{2}} \\ \lesssim & \epsilon h^{-2}\left(\|v^1\|_{0,\omega_j^1\cup\omega_j^2} + \|v^2\|_{0,\omega_j^1\cup\omega_j^2}\right).\end{aligned} \tag{4.10}$$

Therefore,

$$\begin{aligned}\|G_h^1 v^1 - G_h^2 v^2\|_{0,\Omega} \le & \left\|\sum_{j=1}^n (G_h^1 v^1(p_j^1) - G_h^2 v^2)(p_j^2))\phi_j^1\right\|_{0,\Omega} \\ & + \left\|\sum_{j=1}^n (G_h^2 v^2)(p_j^2)(\phi_j^2 - \phi_j^1)\right\|_{0,\Omega} := I_1 + I_2.\end{aligned} \tag{4.11}$$

For I_2, we can use the same argument of (4.8) to show that

$$I_2 \lesssim \epsilon\|G_h^2 v_2\|_{0,\Omega} \lesssim \epsilon\|v_2\|_{1,\Omega} \lesssim \epsilon h^{-1}\|v_2\|_{0,\Omega}.$$

For I_1, by (4.10), we have

$$\begin{aligned}I_1^2 &\le \sum_{j=1}^n |(G_h^1 v^1)(p_j^1) - (G_h^2 v^2)(p_j^2)|^2 |w_j^1| \\ &\lesssim \epsilon^2 h^{-2}(\|v^1\|_{0,\Omega} + \|v^2\|_{0,\Omega})^2.\end{aligned}$$

Combining the estimates for I_1 and I_2, we have

$$\|G_h^1 v^1 - G_h^2 v^2\|_{0,\Omega} \lesssim h^{-1}\epsilon(\|v^1\|_{0,\Omega} + \|v^1\|_{0,\Omega}) \lesssim h^{-1}\epsilon\|v^1\|_{0,\Omega}. \tag{4.12}$$

Now we suppose $\mathcal{T}_h^1$ is a uniform mesh and $\mathcal{T}_h^2$ is a small perturbation such that (4.4) holds for a sufficiently small ϵ. Then for the uniformity of $\mathcal{T}_h^1$, there holds the following *discrete Poincaré inequality*

$$\|G_h^1 v^1\|_{0,\Omega} \gtrsim \|v^1\|_{0,\Omega}, \quad \forall v^1 \in V_{h,0}^1. \tag{4.13}$$

By (4.12),

$$\begin{aligned}\|G_h^2 v^2\|_{0,\Omega} \gtrsim & \|G_h^1 v^1\|_{0,\Omega} - \epsilon h^{-1}\|v^1\|_{0,\Omega} \\ \gtrsim & (1-\epsilon h^{-1})\|v^1\|_{0,\Omega} \gtrsim (1-\epsilon h^{-1})\|v^2\|_{0,\Omega}.\end{aligned} \tag{4.14}$$

When ϵ is sufficient small(significantly smaller than the meshsize), we have the following *discrete Poincaré inequality*

$$\|G_h^2 v^2\|_{0,\Omega} \gtrsim \|v^2\|_{0,\Omega}, \quad \forall v^2 \in V_{h,0}^2. \tag{4.15}$$

Thus assumption (A1) is still valid if the underlying mesh is a small perturbation of a uniform mesh.

5 Numerical Experiments

In this section, we present some numerical tests. Our test results demonstrate that although we have verified (A1) only for some special triangular meshes, our method actually works for many other cases including Chevron, Criss-cross, Unionjack patterns as well as the Delaunay triangulation with regular refinement. For convenience, we denote

$$De := \|u - u_h\|_{0,\Omega}, \qquad D^1 e := |u - u_h|_{1,\Omega},$$
$$D_r^1 e := \|\nabla u - G_h u_h\|_{0,\Omega}, D^2 e := |\nabla u - G_h u_h|_{1,\Omega}$$

for simplicity. In all numerical tests below, we compare two typical gradient recovery operator G_h: polynomial preserving recovery (PPR) and weighted averaging (WA).

Example 1 We consider the following biharmonic equation with homogeneous clamped plate boundary conditions

$$\begin{cases} \Delta^2 u = f \text{ in } \Omega = (0,1) \times (0,1); \\ u = 0 \quad \text{on } \partial\Omega; \\ \frac{\partial u}{\partial n} = 0 \quad \text{on } \partial\Omega; \end{cases} \tag{5.1}$$

with f chosen to fit the exact solution $u(x, y) = x^2(1-x)^2y^2(1-y)^2$.

First, regular pattern uniform triangular mesh is considered and its numerical results are listed in Table 1. As predicted by Theorem 3.2, $D^2 e$ converges at rate of $O(h)$ for both recovered methods. Concerning the H^1 norm error, ∇u_h converges to the exact gradient ∇u at the rate of $O(h)$, while the recovered gradient $G_h u_h$ superconverges at the rate of $O(h^2)$. For the L_2 error, it converges at the rate of $O(h^2)$ which confirms our Theorem 3.4. Note that on the regular pattern uniform triangular mesh, both PPR and WA result in the same stencil in interior domain. However, they are slightly different on the boundary, which explains why we observe some difference between their numerical errors.

Next, we test our scheme on chevron pattern uniform triangular meshes. Notice that the assumption (2.6) fails for the weighted averaging method, which is only a first order finite difference scheme under this mesh. However, (2.6) on arbitrary meshes is guaranteed by the polynomial preserving property (see Theorem 2.2 in [23]) of PPR. For this reason, we list only numerical results in Table 2 for PPR based solver. As predicted by our theory, numerical

Table 1 Numerical results of Example 1 on regular pattern uniform triangular mesh

G_h	Dof	De	Order	$D^1 e$	Order	$D_r^1 e$	Order	$D^2 e$	Order
PPR	1089	4.03e−05	–	6.63e−04	–	1.08e−04	–	4.81e−03	–
PPR	4225	1.07e−05	0.98	2.99e−04	0.59	2.72e−05	1.02	2.25e−03	0.56
PPR	16,641	2.75e−06	0.99	1.45e−04	0.53	6.95e−06	0.99	1.11e−03	0.52
PPR	66,049	6.97e−07	0.99	7.16e−05	0.51	1.77e−06	0.99	5.51e−04	0.51
PPR	263,169	1.76e−07	0.99	3.57e−05	0.50	4.51e−07	0.99	2.75e−04	0.50
WA	1089	1.50e−05	–	1.36e−03	–	5.33e−05	–	5.44e−03	–
WA	4225	3.76e−06	1.02	6.82e−04	0.51	1.31e−05	1.04	2.70e−03	0.52
WA	16,641	9.40e−07	1.01	3.42e−04	0.50	3.23e−06	1.02	1.35e−03	0.51
WA	66,049	2.35e−07	1.01	1.71e−04	0.50	7.99e−07	1.01	6.73e−04	0.50
WA	263,169	5.86e−08	1.00	8.58e−05	0.50	1.96e−07	1.02	3.36e−04	0.50

Table 2 Numerical results of Example 1 on Chevron pattern uniform triangular mesh

G_h	Dof	De	Order	D^1e	Order	D_r^1e	Order	D^2e	Order
PPR	1089	3.40e−05	–	6.40e−04	–	8.48e−05	–	4.83e−03	–
PPR	4225	9.09e−06	0.97	3.21e−04	0.51	2.11e−05	1.03	2.28e−03	0.55
PPR	16,641	2.33e−06	0.99	1.68e−04	0.47	5.42e−06	0.99	1.13e−03	0.51
PPR	66,049	5.92e−07	0.99	8.71e−05	0.48	1.39e−06	0.99	5.61e−04	0.51
PPR	263,169	1.50e−07	0.99	4.47e−05	0.48	3.54e−07	0.99	2.80e−04	0.50

Table 3 Numerical results of Example 1 on Criss-cross pattern uniform triangular mesh

G_h	Dof	De	Order	D^1e	Order	D_r^1e	Order	D^2e	Order
PPR	2113	3.63e−05	–	3.80e−03	–	6.82e−05	–	4.94e−03	–
PPR	8321	9.20e−06	1.00	1.93e−03	0.49	1.75e−05	0.99	2.43e−03	0.52
PPR	33,025	2.28e−06	1.01	8.98e−04	0.56	4.44e−06	0.99	1.19e−03	0.52
PPR	131,585	5.77e−07	0.99	4.63e−04	0.48	1.12e−06	0.99	5.94e−04	0.50
PPR	525,313	1.44e−07	1.00	2.21e−04	0.53	2.87e−07	0.99	2.94e-04	0.51
WA	2113	8.12e−06	–	1.71e−03	–	1.73e−05	–	3.11e−03	–
WA	8321	2.03e−06	1.01	8.56e−04	0.51	4.31e−06	1.01	1.55e−03	0.51
WA	33,025	5.08e−07	1.00	4.28e−04	0.50	1.07e−06	1.01	7.76e−04	0.50
WA	131,585	1.28e−07	1.00	2.14e−04	0.50	2.68e−07	1.00	3.88e−04	0.50
WA	525,313	3.24e−08	0.99	1.07e−04	0.50	6.71e−08	1.00	1.94e−04	0.50

data indicates that the PPR based method converges with numerical error De of order $O(h^2)$, D^1e of order $O(h)$, D_r^1e of order $O(h^2)$, and D^2e of order $O(h)$, respectively.

We also tested Criss-cross and Unionjack pattern uniform triangular meshes and list numerical errors in Tables 3 and 4. Again, we observed $O(h^2)$ for De, $O(h)$ for D^1e, $O(h^2)$ for D_r^1e, and $O(h)$ for D^2e, the same as the regular and Chevron patterns, all agree with our theoretical prediction. It is worth to point out that polynomial preserving recovery and weighted averaging recovery produce different finite element schemes under Criss-cross and Unionjack meshes. Nevertheless, both of them are second order schemes.

Finally, we turn to the Delaunay mesh. The first level coarse mesh is generated by EasyMesh [25] followed by four levels of regular refinement. Table 5 presents the convergence history for the four different errors. For algorithms based on both recovery methods, $O(h^2)$ and $O(h)$ convergence rates are observed for L_2 and H_1 errors, respectively. As for the L_2 error of recovered gradient, $O(h^2)$ superconvergence is observed for polynomial preserving recovery, and $O(h^{1.6})$ for weighted averaging. Regarding the H_2 error, $O(h)$ convergence is observed for polynomial preserved recovery based FEM, and in contrast only $O(h^{0.8})$ convergence is observed for weighted averaging based FEM.

In summary, we see that the polynomial preserving recovery based FEM converges with optimal rates on all four tested uniform meshes as well as the Delaunay mesh.

In order to demonstrate the effectiveness of our method, we make some numerical comparisons with the Morley nonconforming finite element method [21] and the quadratic C^0 interior penalty method [8]. We use the same meshes as before. Tables 6 and 7 list numerical results of the Morley element and the C^0 interior penalty method on the Delaunay triangu-

Table 4 Numerical results of Example 1 on Unionjack pattern uniform triangular mesh

G_h	Dof	De	Order	D^1e	Order	D_r^1e	Order	D^2e	Order
PPR	1089	8.32e−05	–	6.35e−03	–	1.71e−04	–	7.93e−03	–
PPR	4225	2.05e−05	1.03	3.03e−03	0.55	4.39e−05	1.00	3.74e−03	0.55
PPR	16,641	5.04e−06	1.02	1.47e−03	0.53	1.11e−05	1.01	1.78e−03	0.54
PPR	66,049	1.25e−06	1.01	7.21e−04	0.52	2.77e−06	1.00	8.63e−04	0.53
PPR	263,169	3.11e−07	1.01	3.57e−04	0.51	6.95e−07	1.00	4.21e−04	0.52
WA	1089	1.88e−05	–	2.10e−03	–	4.64e−05	–	4.85e−03	–
WA	4225	4.79e−06	1.01	1.07e−03	0.50	1.22e−05	0.98	2.45e−03	0.51
WA	16,641	1.22e−06	1.00	5.39e−04	0.50	3.24e−06	0.97	1.24e−03	0.50
WA	66,049	3.08e−07	1.00	2.72e−04	0.50	8.64e−07	0.96	6.33e−04	0.49
WA	263,169	7.78e−08	0.99	1.37e−04	0.50	2.32e−07	0.95	3.24e−04	0.48

Table 5 Numerical results of Example 1 on Delaunay mesh

G_h	Dof	De	Order	D^1e	Order	D_r^1e	Order	D^2e	Order
PPR	513	8.96e−05	–	1.28e−03	–	2.24e−04	–	7.66e−03	–
PPR	1969	2.27e−05	1.02	5.16e−04	0.68	5.89e−05	0.99	3.62e−03	0.56
PPR	7713	5.74e−06	1.01	2.22e−04	0.62	1.49e−05	1.00	1.69e−03	0.56
PPR	30,529	1.45e−06	1.00	1.05e−04	0.55	3.78e−06	1.00	8.24e−04	0.52
PPR	121,473	3.66e−07	1.00	5.08e−05	0.52	9.60e−07	0.99	4.09e−04	0.51
WA	513	3.67e−05	–	2.71e−03	–	8.37e−05	–	6.69e−03	–
WA	1969	9.07e−06	1.04	1.33e−03	0.53	2.52e−05	0.89	3.51e−03	0.48
WA	7713	2.25e−06	1.02	6.59e−04	0.51	7.87e−06	0.85	1.88e−03	0.46
WA	30,529	5.56e−07	1.02	3.27e−04	0.51	2.54e−06	0.82	1.03e−03	0.44
WA	121,473	1.37e−07	1.02	1.61e−04	0.51	8.43e−07	0.80	5.82e−04	0.41

Table 6 Numerical result of Morley element on Delaunay mesh

Dof	De	Order	D^1e	Order	D^2e	Order
1969	4.29e−05	–	1.41e−04	–	8.94e−03	–
7713	1.08e−05	1.01	3.56e−05	1.01	4.49e−03	0.50
30,529	2.71e−06	1.01	8.93e−06	1.01	2.25e−03	0.50
121,473	6.77e−07	1.00	2.24e−06	1.00	1.12e−03	0.50
484,609	1.69e−07	1.00	5.59e−07	1.00	5.62e−04	0.50

lation with four levels of regular refinement. As expected, both methods demonstrate $O(h)$ convergence rate for the discrete H_2 error and $O(h^2)$ convergence rate for both discrete H_1 error and L_2 error.

From Figs. 2 and 3, we see that the convergent rates of the three methods under the discrete H_2 and H_1 norms are the same while our method has slightly better constants. However, to achieve the same accuracy, our algorithm uses only one-quarter degrees of freedom of the

Table 7 Numerical results of C^0 interior penalty method on Delaunay mesh

Dof	De	Order	D^1e	Order	D^2e	Order
1969	2.04e−05	–	1.01e−04	–	5.67e−03	–
7713	5.46e−06	0.96	2.65e−05	0.98	2.81e−03	0.51
30,529	1.41e−06	0.98	6.78e−06	0.99	1.40e−03	0.51
121,473	3.58e−07	0.99	1.71e−06	1.00	7.00e−04	0.50
484,609	9.04e−08	1.00	4.31e−07	1.00	3.50e−04	0.50

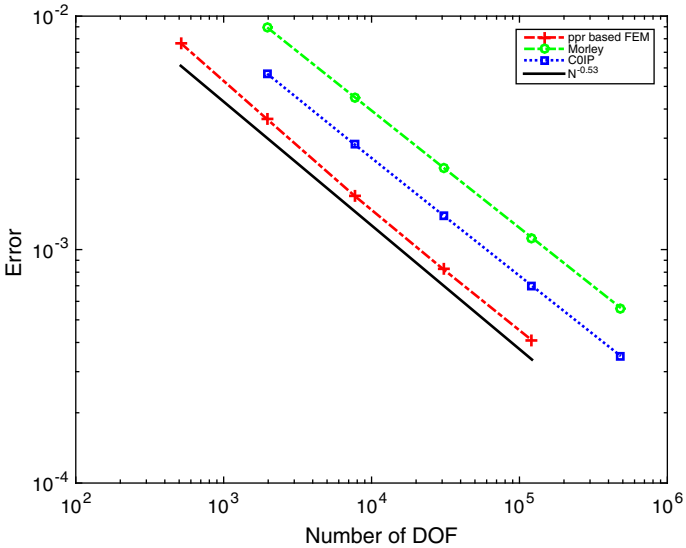

Fig. 2 Comparison of discrete H_2 errors

Morley element and C^0 interior penalty method. In addition, the implementation of our algorithm is much simpler and straightforward.

Example 2 In this example, we consider the following biharmonic equation with simple supported plate boundary condition

$$\begin{cases} \Delta^2 u = f, & \text{in } \Omega = (0,1) \times (0,1); \\ u = 0, & \text{on } \partial\Omega; \\ \frac{\partial^2 u}{\partial \mathbf{n}^2} = g, & \text{on } \partial\Omega; \end{cases} \tag{5.2}$$

with f chosen to fit the exact solution $u(x, y) = x^2(1-x)^2y^2(1-y)^2$. The boundary function g is given by

$$g = \mathbf{n}^{\mathsf{T}} \begin{bmatrix} 2(6x^2-6x+1)y^2(1-y)^2 & 4(2x^3-3x^2+x)(2y^3-3y^2+y) \\ 4(2x^3-3x^2+x)(2y^3-3y^2+y) & 2x^2(1-x)^2(6y^2-6y+1) \end{bmatrix} n;$$

with $\mathbf{n}$ being a unit out normal vector on the boundary $\partial\Omega$.

As in Example 1, we first test our algorithms on regular pattern uniform triangular mesh and list the numerical results in Table 8. Again, we observe optimal convergence rates of the

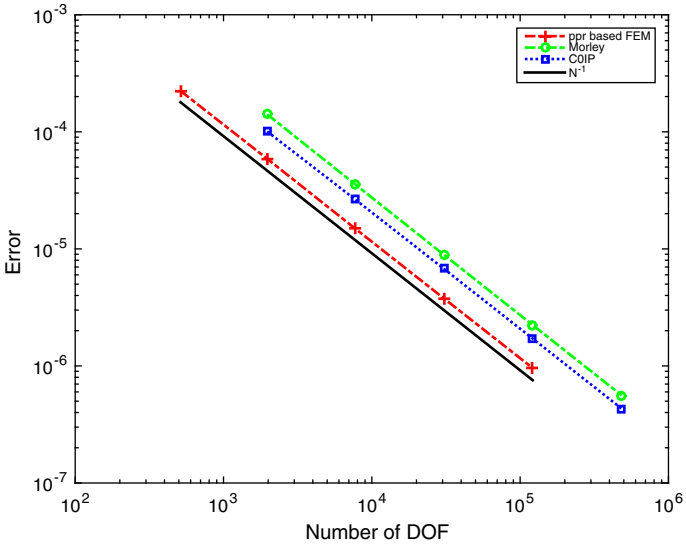

Fig. 3 Comparison of discrete H_1 errors

Table 8 Numerical results of Example 2 on regular pattern uniform triangular mesh

G_h	Dof	De	Order	D^1e	Order	D_r^1e	Order	D^2e	Order
PPR	1089	3.35e−05	–	6.98e−04	–	7.79e−05	–	4.65e−03	–
PPR	4225	8.53e−06	1.01	3.04e−04	0.61	1.96e−05	1.02	2.25e−03	0.54
PPR	16,641	2.15e−06	1.00	1.45e−04	0.54	4.91e−06	1.01	1.11e−03	0.52
PPR	66,049	5.41e−07	1.00	7.16e−05	0.51	1.23e−06	1.00	5.51e−04	0.51
PPR	263,169	1.36e−07	1.00	3.57e−05	0.50	3.08e−07	1.00	2.75e−04	0.50
WA	1089	2.80e−05	–	1.38e−03	–	9.21e−05	–	5.39e−03	–
WA	4225	6.99e−06	1.02	6.88e−04	0.51	2.31e−05	1.02	2.69e−03	0.51
WA	16,641	1.75e−06	1.01	3.43e−04	0.51	5.77e−06	1.01	1.34e−03	0.51
WA	66,049	4.37e−07	1.01	1.72e−04	0.50	1.44e−06	1.01	6.72e−04	0.50
WA	263,169	1.09e−07	1.00	8.58e−05	0.50	3.60e−07	1.00	3.36e−04	0.50

H^2 error D^2e, the H^1 error D^1e, the H^1 recovery error D_r^1e and the L^2 error De for both the PPR and WA based algorithms.

We then consider chevron pattern uniform triangular mesh. Due to the same reason in the previous example, we only list numerical results for PPR based solver in Table 9. It clearly indicates that u_h converges to u with a rate of $O(h^2)$ under the L^2 norm, at a rate of $O(h)$ under both the H^1 norm and H^2 norm. Moreover, the recovery gradient $G_h u_h$ converges to ∇u at a rate of $O(h^2)$. We also test our algorithms on Delaunay meshes as in the previous example. The numerical results are listed in Table 10. Similar to what we observed in regular pattern uniform triangular mesh, both methods converge with optimal convergence rate .

In addition, we have tested our algorithms on other two types(Criss-cross and Unionjack pattern) uniform triangular meshes. Since the numerical results are similar to the corresponding parts in the previous example, they are not reported here.

Table 9 Numerical results of Example 2 on chevron pattern uniform triangular mesh

G_h	Dof	De	Order	D^1e	Order	D_r^1e	Order	D^2e	Order
PPR	1089	2.58e−05	–	8.94e−04	–	5.55e−05	–	4.82e−03	–
PPR	4225	6.69e−06	0.99	5.01e−04	0.43	1.41e−05	1.01	2.38e−03	0.52
PPR	16,641	1.72e−06	0.99	2.89e−04	0.40	3.67e−06	0.98	1.20e−03	0.50
PPR	66,049	4.46e−07	0.98	1.71e−04	0.38	9.77e−07	0.96	6.14e−04	0.48
PPR	263,169	1.17e−07	0.97	1.04e−04	0.36	2.69e−07	0.93	3.22e−04	0.47

Table 10 Numerical results of Example 2 on Delaunay mesh

G_h	Dof	De	Order	D^1e	Order	D_r^1e	Order	D^2e	Order
PPR	513	7.57e−05	–	1.36e−03	–	1.88e−04	–	8.19e−03	–
PPR	1969	1.83e−05	1.06	5.29e−04	0.70	4.53e−05	1.06	3.77e−03	0.58
PPR	7713	4.48e−06	1.03	2.24e−04	0.63	1.06e−05	1.06	1.73e−03	0.57
PPR	30,529	1.11e−06	1.01	1.05e−04	0.55	2.58e−06	1.03	8.32e−04	0.53
PPR	121,473	2.77e−07	1.01	5.09e−05	0.52	6.40e−07	1.01	4.11e−04	0.51
WA	513	5.49e−05	–	2.70e−03	–	1.62e−04	–	6.68e−03	–
WA	1969	1.36e−05	1.04	1.33e−03	0.53	4.25e−05	0.99	3.51e−03	0.48
WA	7713	3.34e−06	1.03	6.59e−04	0.51	1.15e−05	0.96	1.88e−03	0.46
WA	30,529	8.13e−07	1.03	3.27e−04	0.51	3.20e−06	0.93	1.03e−03	0.44
WA	121,473	1.93e−07	1.04	1.61e−04	0.51	9.45e−07	0.88	5.82e−04	0.41

Finally, we numerically compare PPR based algorithm with the Morley nonconforming finite element method and C^0 interior penalty method. Depicted in Figs. 4 and 5 are their comparisons. Again we clearly observe that all these three methods converge with the same rates and PPR based method is more computationally efficient than both the Morley element and C^0 interior penalty method.

Example 3 In all the previous numerical examples, the solutions are analytic. Here we consider biharmonic equation

$$-\Delta^2 u = 0$$

on the L-shaped domain $\Omega = (-1, 1) \times (-1, 1) \setminus (0, 1) \times (-1, 0)$ with the exact solution $u = r^{\frac{5}{3}} sin(\frac{3}{5}\theta)$. The corresponding clamped plate boundary conditions are computed from u. Note the u has a singularity at the original. The solution $u \in H^{\frac{8}{3}-\epsilon} \notin H^3(\Omega)$ We firstly use the C^0 FEM to solve it on the uniform mesh as plotted in Fig. 6a. Table 11 lists it numerical results for PPR. The method does converge with the suboptimal order $h^{\frac{2}{3}}$ in the discrete H^2 norm due to the singularity. To resolve the singularity, we also use the graded mesh with graded parameter $\kappa = 0.2$ generated by LGN_FEM [20]. The initial mesh is shown is Fig. 6b. We reports the numerical results it Table 12. Clearly, we obtain optimal convergence rate in all different norms.

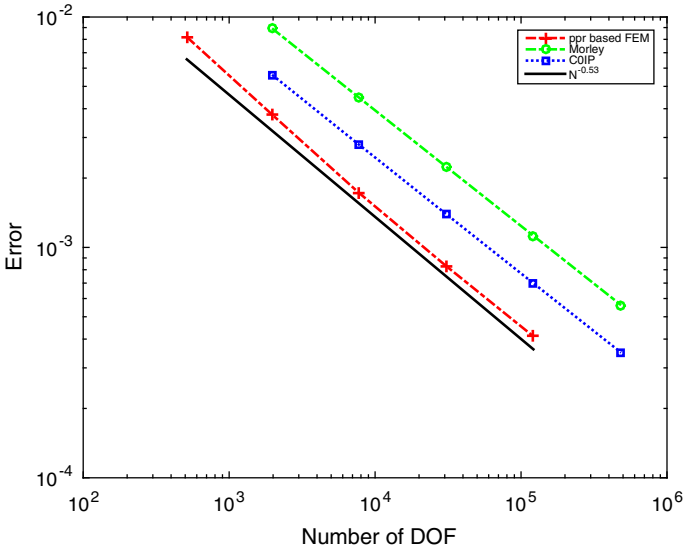

Fig. 4 Comparison of discrete H_2 errors for Example 2

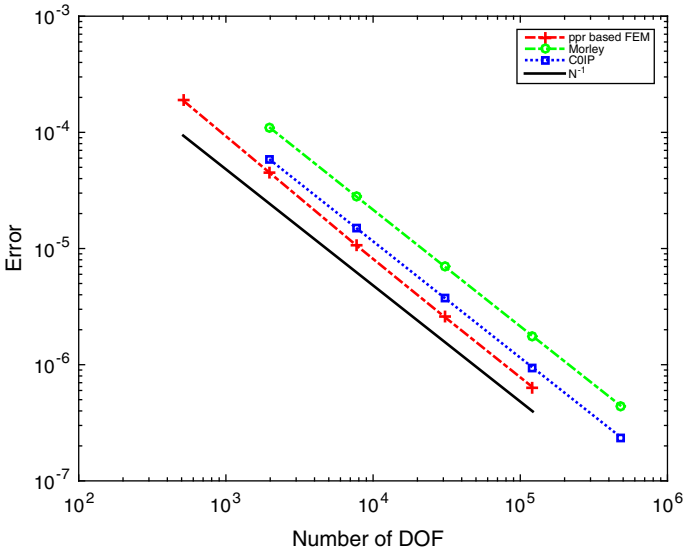

Fig. 5 Comparison of discrete H_1 errors for Example 2

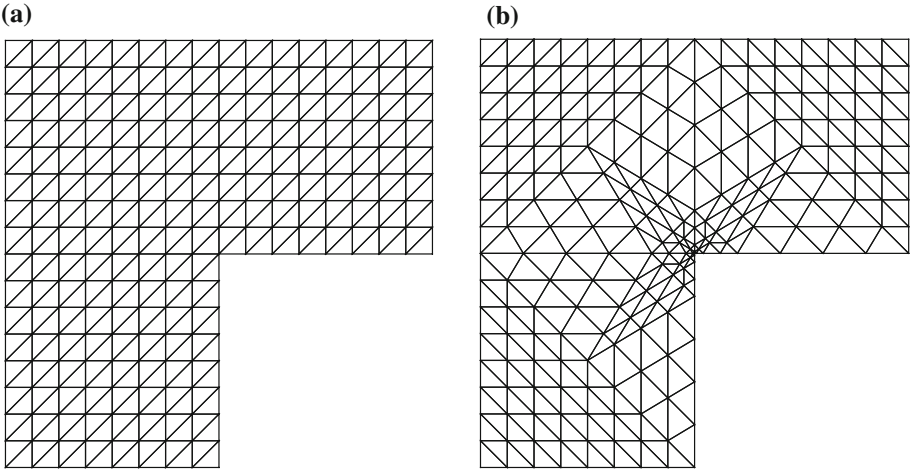

Fig. 6 Meshes for L-shape domain: **a** uniform mesh, **b** graded mesh

Table 11 Results of Example 3 on uniform mesh

Dof	De	Order	D^1e	Order	D_r^1e	Order	D^2e	Order
225	2.06e−02	–	1.94e−01	–	6.81e−02	–	5.93e−01	–
833	7.15e−03	0.81	9.93e−02	0.51	2.63e−02	0.73	3.31e−01	0.45
3201	2.72e−03	0.72	5.45e−02	0.45	1.08e−02	0.66	1.98e−01	0.38
12,545	1.08e−03	0.68	3.02e−02	0.43	4.48e−03	0.64	1.21e−01	0.36
49,665	4.40e−04	0.65	1.66e−02	0.43	1.87e−03	0.63	7.46e−02	0.35
197,633	1.82e−04	0.64	9.15e−03	0.43	7.86e−04	0.63	4.63e−02	0.35

Table 12 Results of Example 3 on graded mesh

Dof	De	Order	D^1e	Order	D_r^1e	Order	D^2e	Order
225	3.95e−03	–	1.48e−01	–	7.55e−03	–	1.67e−01	–
833	8.88e−04	1.14	7.32e−02	0.54	1.83e−03	1.08	8.13e−02	0.55
3201	2.16e−04	1.05	3.65e−02	0.52	4.66e−04	1.02	4.13e−02	0.50
12,545	5.34e−05	1.02	1.83e−02	0.51	1.18e−04	1.01	2.10e−02	0.49
49,665	1.32e−05	1.01	9.12e−03	0.50	2.95e−05	1.01	1.06e−02	0.50
197,633	3.28e−06	1.01	4.56e−03	0.50	7.34e−06	1.01	5.35e−03	0.50

6 Concluding Remarks

In this paper, we present and analyze a recovery based linear finite element method for biharmonic problems. The method circumvents the complicated C^1 conforming FEMs, and uses only values at element vertices as degrees of freedom, and hence is much simpler and more efficient than non-conforming finite elements. The scheme has been proved to converge with optimal rates in L^2, H^1, and discrete H^2 norms. Moreover, if we apply the

gradient recovery operator to post-process the numerical solution, the recovered gradient is superconvergent to the exact one. Numerical comparison with the Morley nonconforming element and the C^0 interior penalty method indicate that to achieve the same accuracy, our method requires only one-quarter degrees of freedom of the other two methods. As a continue of this study, we have applied the proposed finite element method to efficiently solving two fourth-order eigenvalue problems in [14].

Finally, we would like to indicate that the idea in this paper can be applied to construct efficient schemes for other higher-order differential equations and some nonlinear problems. In fact, solving the Monge–Ampere equation (a fully nonlinear case) by the recovery based linear finite element method is one of our ongoing research projects.

References

1. Adini, A., Clough, R.W.: Analysis of plate bending by the finite element method, NSF report G. 7337 (1961)
2. Ainsworth, M., Oden, J.T.: A Posteriori Error Estimation in Finite Element Analysis. Wiley Interscience, New York (2000)
3. Babuska, I., Strouboulis, T.: The Finite Element Method and Its Reliability. Oxford University Press, London (2001)
4. Bank, R.E., Weiser, A.: Some a posteriori error estimators for elliptic partial differential equations. Math. comp. **44**, 283–301 (1985)
5. Bank, R.E., Xu, J.: Asymptotically exact a posteriori error estimators, Part I: Grid with superconvergence. SIAM J. Numer. Anal. **41**, 2294–2312 (2003)
6. Baker, G.A.: Fintie element methods for elliptic equations using nonconforming elements. Math. Comp. **31**, 45–59 (1977)
7. Bank, R.E., Xu, J.: Asymptotically exact a posteriori error estimators, Part II: general unstructured grids. SIAM J. Numer. Anal. **41**, 2313–2332 (2003)
8. Brenner, S., Sung, L.: C0 interior penalty methods for fourth order elliptic boundary value problems on polygonal domains. J. Sci. Comput. **22/23**, 83–118 (2005)
9. Brenner, S., Scott, L.R.: Mathematical Theory of Finite element Methods, 3rd edn. Spriger-Verlag, New York (2008)
10. Ciarlet, P.G.: The Finite Element Method for Elliptic Problems, Studies in Mathematics and its Applications, vol. 4. North-Holland, Amsterdam (1978)
11. COMSOL Multiphysics 3.5a User's Guide, p. 471 (2008)
12. Introduction to COMSOL Multiphysics Version 5.1, p. 46 (2015)
13. Chatelin, Francoise: Spectral Approximation of Linear Operators, Computer Science and Applied Mathematics. Academic Press Inc., New York (1983)
14. Chen, H., Guo, H., Zhang, Z., Zou, Q.: A C^0 Linear Finite Element Method For Two Fourth-Order Eigenvalue Problems IMA. J. Numer. Anal. (2016). doi:10.1093/imanum/drw051
15. Guo, H., Zhang, Z., Zhao, R., Zou, Q.: Polynomial preserving recovery on boundary. J. Comput. Appl. Math. **307**, 119–133 (2016)
16. Guo, H., Yang, X.: Polynomial preserving recovery for high frequency wave propagation. J. Sci. Comput. **71**, 594–614 (2017)
17. El-Gamel, M., Sameeh, M.: An efficient technique for finding the eigenvalues of fourth-order Sturm–Liouville problems. Appl. Math. **3**, 920–925 (2012)
18. Lamichhane, B.: A stabilized mixed finite element method for the biharmonic equation based on biorthogonal systems. J. Comput. Appl. Math. **235**, 5188–5197 (2011)
19. Lamichhane, B.: A finite element method for a biharmonic equation based on gradient recovery operators. BIT Numer. Math. **54**, 469–484 (2014)
20. Li, H., Nistor, V.: LNG_FEM: graded meshes on domains of polygonal structures. Rec. Adv. Sci. Comput. Appl. **586**, 239–246 (2013)
21. Morley, L.: The triangular equilibrium problem in the solution of plate bending problems. Aero. Quart. **19**, 149C–169 (1968)
22. Naga, A., Zhang, Z.: A posteriori error estimates based on the polynomial preserving recovery. SIAM J. Numer. Anal. **42–4**, 1780–1800 (2004)

23. Naga, A., Zhang, Z.: The polynomial-preserving recovery for higher order finite element methods in 2D and 3D. Discret. Contin. Dyn. Syst.-Ser. B **5–3**, 769–798 (2005)
24. Naga, A., Zhang, Z.: Function value recovery and its application in eigenvalue problems. SIAM J. Numer. Anal. **50**, 272–286 (2012)
25. Niceno, B.: EasyMesh Version 1.4: A two-dimensional quality mesh generator. http://www-dinma.univ.trieste.it/nirftc/research/easymesh
26. Wang, M., Xu, J.: The Morley element for fourth order elliptic equations in any dimensions. Numer. Math. **103**, 155–169 (2006)
27. Xu, J., Zhang, Z.: Analysis of recovery type a posteriori error estimators for mildly structured grids. Math. Comp. **73**, 1139–1152 (2004)
28. Zhang, S., Zhang, Z.: Invalidity of decoupling a biharmonic equation to two Poisson equations on non-convex polygons. Int. J. Numer. Anal. Model. **5**, 73–76 (2008)
29. Zhang, Z.: Recovery Techniques in Finite Element Methods. In: Tang, T., Xu, J. (eds.) Adaptive Computations: Theory and Algorithms. Mathematics Monograph Series 6, pp. 333–412. Science Publisher, London (2007)
30. Zhang, Z., Naga, A.: A new finite element gradient recovery method: superconvergence property. SIAM J. Sci. Comput. **26–4**, 1192–1213 (2005)
31. Zienkiewicz, O.C., Zhu, J.Z.: The superconvergence patch recovery and a posteriori error estimates part 1: the recovery technique. Int. J. Numer. Methods Eng. **33**, 1331–1364 (1992)